Journal of Wind Engineering & Industrial Aerodynamics 201 (2020) 104185

Contents lists available at ScienceDirect

Journal of Wind Engineering & Industrial Aerodynamics

journal homepage: www.elsevier.com/locate/jweia

The impact of atmospheric boundary layer, opening configuration and presence of animals on the ventilation of a cattle barn

Štěpán Nosek [a,*], Zuzana Kluková [a,b], Michala Jakubcová [a], Qianying Yi [c], David Janke [c], Peter Demeyer [d], Zbyněk Jaňour [a]

[a] Institute of Thermomechanics AS CR, v.v.i., Dolejškova 1402/5, Prague 8, 182 00, Czech Republic
[b] Charles University, Faculty of Mathematics and Physics, Department of Atmospheric Physics, V Holešovičkách 2, Prague, Czech Republic
[c] Department of Engineering for Livestock Management, Leibniz Institute for Agricultural Engineering and Bioeconomy (ATB), Max-Eyth-Allee 100, 14469, Potsdam, Germany
[d] Technology and Food Science Unit - Agricultural Engineering, Institute for Agricultural and Fisheries Research (ILVO), Burg. Van Gansberghelaan 115 bus 1, 9820, Merelbeke, Belgium

ARTICLE INFO

Keywords:
Air pollution
Atmospheric boundary layer
Livestock building
Natural ventilation
OPD
TR-PIV
Wind tunnel

ABSTRACT

Naturally ventilated livestock buildings (NVLB) represent one of the most significant sources of ammonia emissions. However, even the dispersion of passive gas in an NVLB is still not well understood. In this paper, we present a detailed investigation of passive pollutant dispersion in a model of a cattle barn using the wind tunnel experiment method. We simulated the pollution of the barn by a ground-level planar source. We used the time-resolved particle image velocimetry (TR-PIV) and the fast flame ionisation detector (FFID) to study the flow and dispersion processes at high spatial and temporal resolution. We employed the Proper Orthogonal Decomposition (POD) and Oscillating Patterns Decomposition (OPD) methods to detect the coherent structures of the flow. The results show that the type of atmospheric boundary layer (ABL) and sidewall opening height have a significant impact on the pollutant dispersion in the barn, while the presence of animals and doors openings are insignificant under conditions of winds perpendicular to the sidewall openings. We found that the dynamic coherent structures, developed by the Kelvin-Helmholtz instability, contribute to the pollutant transport in the barn. We demonstrate that in any of the studied cases the pollutant was not well mixed within the barn and that a significant underestimation (up to by a factor 3) of the barn ventilation might be obtained using, e.g. tracer gas method.

1. Introduction

Naturally ventilated livestock buildings (NVLB), such as cattle barns, represent one of the most significant sources of ammonia emissions. While higher concentrations of ammonia pose severe health and environmental issue (Krupa, 2003), the dispersion processes even of passive pollutant within NVLBs are still not well understood (Bjerg et al., 2013). Previous studies (Arogo et al., 1999; De Paepe et al., 2016; Olesen and Sommer, 1993; Rong et al., 2009) observed that higher air velocity and turbulence above the manure or slurry surface resulted in higher ammonia emissions. However, the prediction of the flow velocity and turbulence close to these surfaces is not trivial. NVLBs have relatively large openings, and due to these openings, a complex interaction of outdoor flows with the indoor environment occurs. Moreover, the weather diurnal cycles and heterogeneity of the earth surface produces unsteady turbulent flow around an NVLB, and it is impossible by current measurement techniques to obtain characteristic flow patterns or concentrations within such buildings from field experiments (Schatzmann and Leitl, 2011).

Therefore, previous studies used computational fluid dynamics (CFD) simulations (e.g., Norton et al., 2009; Rong et al., 2015; Shen et al., 2013; Wu et al., 2012; Yi et al., 2019) or wind-tunnel experiments (e.g., Choiniere et al., 1988; De Paepe et al., 2013; Fiedler et al., 2013; Ikeguchi et al., 2005; Shen et al., 2016; Yi et al., 2018) to understand the flow patterns generated within an NVLB. CFD can solve the problem concerning all processes (mechanical, thermodynamic and chemical) involved without similarity constraints. However, CFD simulations are not trustworthy before their validation due to the inherent complexity of turbulent flow and the need for its parametrisation. This parametrisation has a higher impact on the accuracy of the pollutant concentration

* Corresponding author.
E-mail address: nosek@it.cas.cz (Š. Nosek).

https://doi.org/10.1016/j.jweia.2020.104185
Received 7 January 2020; Received in revised form 17 March 2020; Accepted 2 April 2020
Available online 16 April 2020

prediction, and hence the validation of the flow does not guarantee a correct prediction of the pollutant dispersion (Schatzmann et al., 2010).

A wind-tunnel modelling does not suffer from such ambiguity since it can employ a real flow and real pollutant. The conditions can be fully controlled and statistically steady, which provides representative and reproducible data. However, wind tunnel modelling encounters similarity criteria fulfilment, and hence hardly simulates all processes involved in the scaled-down phenomenon. Due to the reduction of the Reynolds number, wind tunnels cannot model the smallest eddies at so-called Kolmogorov length scale (which is about 1 mm at full-scale) occurring in the atmospheric boundary layer (ABL). However, the most energy-containing eddies which play the most important role in the dispersion of pollutant within ABL are those which are bigger than the Kolmogorov length scale Snyder, 1981. Therefore, wind tunnel modelling remains a reliable research tool to study flow and dispersion processes occurring in the lowest part of the atmosphere (ABL).

Previous wind-tunnel studies show that the geometry of sidewall openings has a crucial impact on the flow patterns (Ikeguchi et al., 2003; Morsing et al., 2002; Yi et al., 2018a) and ventilation (De Paepe et al., 2013; Shen et al., 2016; Yi et al., 2019) of NVLB. However, none of these studies included doors openings or the presence of animals into their models. The increase of the opening size results in the increase of the airspeed and turbulent kinetic energy within an NVLB but also the increase of the discharge coefficient of the opening (Yi et al., 2018b). De Paepe et al. (2013) and Shen et al. (2016) demonstrated that different positions of the inlet and outlet openings also has important effect on the airspeed within their model of a cattle barn. However, both these studies did not investigate airflow patterns in detail.

Morsing et al. (2002) and Yi et al. (2018a) observed 'up-jet' airflow patterns with a recirculation zone positioned in the lower portion of the cattle barn model. Yi et al. (2018a) demonstrated these patterns for the opening sizes which had an opening ratio (opening area divided by the sum of the opening and wall area) smaller than 62.71% and which were positioned just below the eaves. That study also shows that a 'lower' openings configuration (positioned just above the cattle bottom) produced an airflow jet in the lower part of the barn and an air recirculation in the upper part of the barn.

Tominaga and Blocken, 2015 observed in their study on a cross-ventilated generic building that the pollutant dispersion is mainly driven by the concentration gradient and not by the mean characteristics of the turbulent flow (e.g., turbulent kinetic energy). Therefore, studying only these flow characteristics does not guarantee the understanding of the pollutant dispersion within NVLBs. However, only a few studies on NVLBs take into account a pollutant. Zhang et al. (2003) studied obstacle effects on airflow and CO2 dispersion around the model of a cattle barn. Their results showed that the obstacle situated at the upstream of the building decreased the downstream CO2 concentration. Later, Ikeguchi et al. (2005) observed that air contaminated by a passive gas (ethylene) might reach the upwind livestock building even if it was generated in the downwind building. This phenomenon was observed when the buildings were placed at a separation distance equal to their average height. However, this was observed for one opening configuration, and concentration patterns were not investigated by that study.

Interestingly, there is no study which addresses the impact of different ABLs on the flow or the pollutant dispersion within an NVLB. Indeed, the ABL might drive the pollutant dispersion inside an NVLB primarily due to its large openings. Findings of Ramponi and Blocken (2012) show that the turbulent kinetic energy of the approaching flow affects the direction of the incoming jet through the inlet opening of the generic building significantly. Another limitation of previous wind-tunnel studies on NVLB ventilation is that they did not take into account the presence of animals or doors openings in their building models, although a significant impact of these parameters on the flow and pollutant dispersion within NVLB might be expected (height of the animals and doors openings are approximately 0.2 and 0.5 of NVLB height, respectively).

This paper addresses the limitations mentioned above to understand better the dispersion processes in an NVLB. Therefore, the main objectives of the present study are the following: i) to study the impact of ABL on both the flow and pollutant dispersion in a cattle barn with respect to the presence of animals and doors openings; ii) to evaluate the role of coherent structures on the pollutant dispersion within the barn; iii) to exploit principles of physical modelling in a wind tunnel and state-of-the-art measuring and analytical methods for the accomplishment of these objectives.

2. Methods

2.1. Experimental setup

The experiments were performed in the Environmental wind tunnel of the Institute of Thermomechanics of the Czech Academy of Sciences. It is an open wind tunnel with cross dimensions of 1.5 m × 1.5 m, and the lengths of the development and test sections are 20.5 m and 2 m, respectively. The air is sucked from the outdoors within a range of 0.1–10 m s-1 by a fan, which is driven through a frequency converter with an accuracy of 0.05 m s-1. Considering the fulfilment of the internal Reynolds number independence (Cermak et al., 1984) on the flow within a model of a cattle barn (25 m in length, 20 m in width and 9.5 m in height) and the dimensions of the wind tunnel, the scale ratio of the model resulted in 1:50. The model was positioned at the centre of the wind-tunnel test section and has lower blockage ratio (the ratio of the frontal area of the model to the area of the wind-tunnel cross-section) than 5% (Fig. 1a).

To observe the impact of ABL on the ventilation of the model, two types of ABL were simulated in the tunnel. The first corresponded to a moderately rough (e.g., rural) and the second to a very rough (e.g., forest) terrain. Both ABLs were developed by vortex (spires) and turbulence (thin rectangular plates) generators at the development section. While three spires (isosceles trapezoids which were of 625 and 85 mm in bases and 1420 mm in height, see Fig. 1a) initiated the rural ABL, four of these spires started the forest ABL. In the case of the rural ABL, it was found that a barrier wall 0.5 m upwind of the spires is essential to reproduce appropriate integral length scales of turbulence in the measurement section for the given scale. Indeed, there was also a difference in the turbulence generators between these two cases of modelled ABL. Both ABLs turbulence generators were rectangle thin plates of the same width (50 mm) and were positioned at a staggered pattern along the remaining part of the development section, but the rural ABL had these generators of 10 mm and the forest ABL of 100 mm in height. The generators also differed at the streamwise position; they were deployed every 500 mm in the case of the rural ABL (Fig. 1a), and every 250 mm in the case of the forest ABL (not shown). The vertical profiles of the mean dimensionless longitudinal velocity and turbulence intensities (together with the bounds recommended by VDI, 2000) of both simulated ABLs were scaled up by 50:1 (the measured height in the wind tunnel was multiplied by 50) and are presented in Fig. 2a. The profiles were measured 750 mm (approx. equal to $4H$, where H is the height of the cattle barn model) upwind of the centre of the test section by a 2D laser Doppler anemometry (LDA) from Dantec Dynamics. The average sampling frequency was about 500 Hz, and the duration of the measurement at each point was 90 s. For both profiles and during the entire measuring campaign, the freestream velocity (hereafter the reference velocity, U_{ref}) of 5.4 m/s was used as the reference velocity for the normalisation of results, and maintained in the wind tunnel and measured by the Prandtl tube (Fig. 1a) about 1 m above the tunnel floor (the model-scale boundary thickness was about the same height).

In Fig. 2b and 2c, the spectra and integral length scales of turbulence of the streamwise velocity (L_{ux}), computed from time series measured at height 580 mm (29 m at full-scale) are presented, while L_{ux}s examined for another two lower heights (480 mm and 195 mm which correspond to 24 m and 9 m at full-scale, respectively) are presented only in Fig. 2c. The

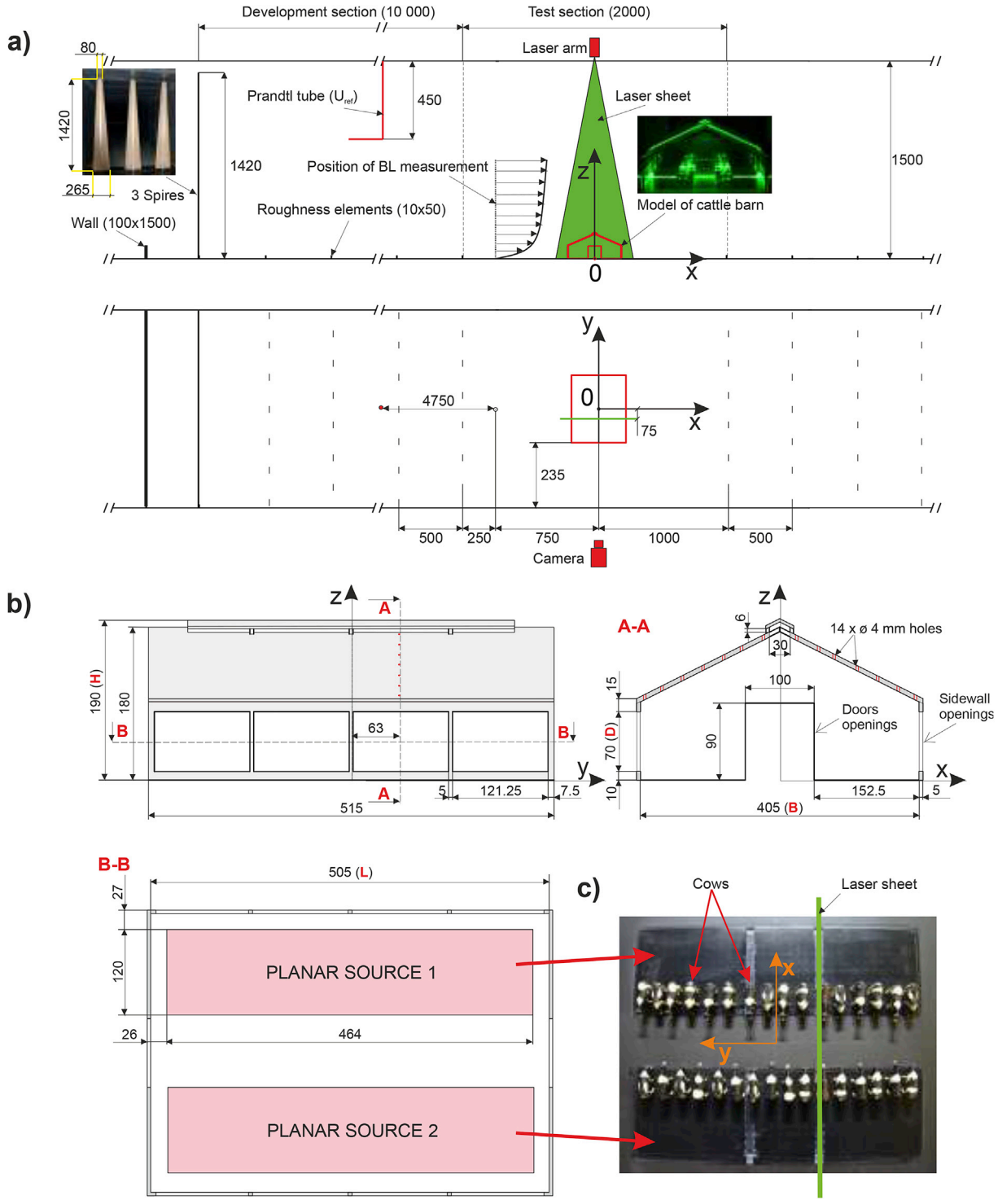

Fig. 1. a) Schemas of the experimental setup for development of rural ABL and PIV measurement of the vertical plane within the model of cattle barn in the wind tunnel (top: side view, bottom: top view); **b)** schemas of the cattle barn and planar source models; **c)** snapshot (from the top) of the positions of cow models inside the model of the cattle barn (the model of the cattle barn is not shown for the sake of clarity). All dimensions are in mm.

spectra are compared with the semi-empirical model from von Karmán, and the integral length scales are compared with those recommended by Counihan (1975). From these figures, one can observe that both the spectrum and integral length scale of turbulence were modelled appropriately in the wind tunnel for both simulated ABLs at full-scale height 29 m. However, for the lower heights (especially that at 9 m) it was hard to achieve such long L_{ux}s as those recommended by Counihan (1975). This clearly shows on limitation of the wind-tunnel to model L_{ux} close to the ground for such small scales (here 1:50). However, the other important parameters of ABLs' velocity profiles (the velocity profile exponent, α, the friction velocity, u_*, the roughness length, z_0, and the displacement height, d_0) were simulated according to VDI (2000) (with the exception for the very rough ABL, where a rather low d was achieved) and are summarised in Table 1.

While the model of the cattle barn was designed as simple as possible, all critical geometrical features (the roof ridge, opening geometry, and

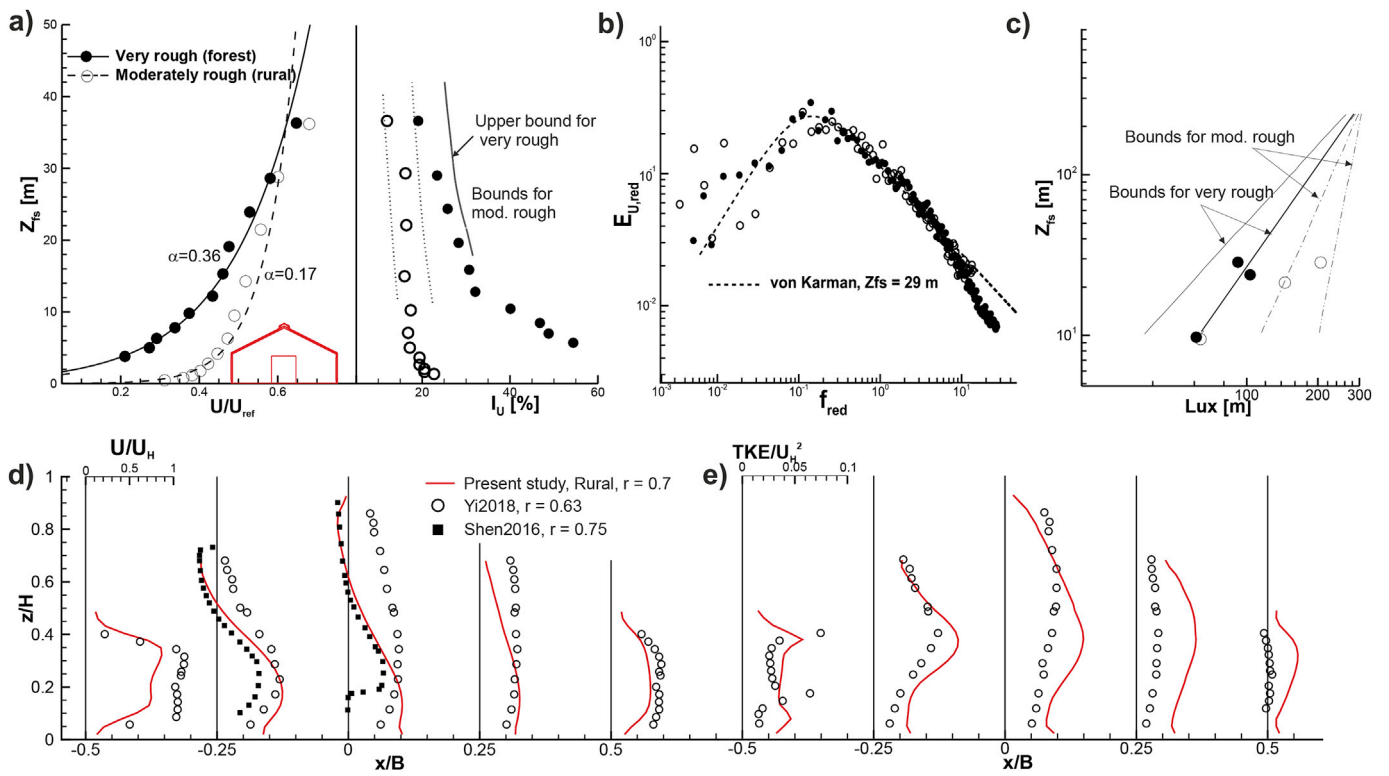

Fig. 2. Vertical profiles of the streamwise **(a)** mean dimensionless velocity (U/U_{ref}) and turbulence intensity (I_u) of the simulated very (*filled circles*) and moderately (*open circles*) rough ABL accompanied with the recommended power exponents (α) and bounds for I_u according to VDI (2000); **(b)** turbulence spectra at full-scale height z_{fs} = 29 m of the simulated ABLs and their comparisons with semi-empirical model according to von Karmán; **(c)** integral length scale of turbulence (L_{ux}) computed at three full-scale heights of the simulated ABLs accompanied with the recommended bounds by VDI (2000); **(d)** comparison of the vertical profiles of the dimensionless mean streamwise velocity (U/U_H) and **(e)** turbulent kinetic energy (TKE/U_H) at six streamwise positions ($x/B = -0.48, -0.25, 0, 0.25$ and 0.48) within the model of cattle barn between the present study (*red solid lines*) simulated for the rural terrain and the study of Yi et al. (2018a) (*open circles*) and Shen et al. (2016) (*filled squares*). The full-scale heights (z_{fs}) in **(a–c)** were scaled up by 50:1. (For interpretation of the references to colour in this figure legend, the reader is referred to the Web version of this article.)

Table 1
Overview of the studied cases.

Config.	Terrain Roughness	ABL parameters	Openings	Opening height, D [mm]	Porosity, r	Doors
R1	Moderately rough - Rural	$\alpha = 0.17$, $u_* = 0.25$ m/s, $z_0 = 0.01$ m, $d_0 = 0$ m,	Fully Open	70	0.70	Open Closed
R2			1/2 Open	35	0.35	Open Closed
R4			1/4 Open	17.5	0.17	Open Closed
F1, F2 and F4	Very rough - Forest	$\alpha = 0.36$, $u_* = 0.45$ m/s, $z_0 = 0.5$ m, $d_0 = 2$ m,	The same as in the case of the rural terrain			

ABL parameters were scaled up by 50:1.

doors) of a typical cattle barn were reproduced (Fig. 1b). To the best of the authors' knowledge, this was the first time where the doors openings and pillars at the sidewall openings were included in the model as well. The studied sidewall opening configurations reflected three regimes of the natural ventilation under isothermal conditions. The first corresponded to summer regime, and hence the openings were left fully open (D = 70 mm, Fig. 1b) at both sidewalls. The second corresponded to autumn/spring regime with the half-open openings (D = 35 mm), and the third to winter regime with the quarter-open openings (D = 17.5 mm), at both sidewalls. These three regimes also reflected the porosity of the sidewalls (r = 0.7, 0.35 and 0.175, respectively) oriented perpendicularly to the approach wind. For all these regimes, the effect (open or closed) of doors openings (100 mm in height and 90 mm in width) and the presence of the animals on the flow were studied as well (see Table 1). The models of cows (KidsGlobe company) were made of plastic and scale of 1:50. In total, 24 configurations were studied. However, due to the financial costs and time, the cases with closed doors were excluded from the concentration measurements.

The pollution of the cattle barn was simulated using two ground-level planar sources, which emitted the passive gas (ethane) homogeneously (Fig. 1b and c). Indeed, the ammonia is not a passive gas (it is a buoyant and reactive compound with a density of 0.73 kg m^{-3} at 1.013 bar and 15 °C). Hence, one may expect an overestimation in the observed concentrations within the model of the barn due to the buoyancy. However, to reduce the complexity of the problem, ethane was chosen as a first approximation in the present study. The authors used their previous experience with modelling of pollution from traffic in the wind tunnel (Nosek et al., 2017) to design the planar source for this study. Therefore, the ethane was emitted through 288 tubes at each of the sources. The tubes had an inner diameter of 0.5 mm and length of 30 mm, and they were incorporated into the plenum chamber, which was positioned below the wind-tunnel bottom. The entire lengths of the tubes were

positioned vertically and below the bottom of the cattle barn model with their outlets facing that bottom. Such geometry of the tubes made the ethane flow rate of 10.4 ml s^{-1} insensitive to the local pressure fluctuations of the cattle barn (Meroney et al., 1996). The homogeneity of the sources and the influence of their ethane discharge velocity on the cattle barn flow were tested by several measurements and visualisation tests (both performed by PIV system) before the measurement campaign. The lowest internal Reynolds number $Re_i = U_i L_i/\nu = 22430$, where U_i is the maximum velocity within the building (which is usually equal to the velocity at the opening and L_i is the smallest internal dimension of the barn (which is usually the eaves height) was checked as well. Cermak et al. (1984) demonstrated on a building model with a scale of 1:25 that the internal Reynolds should be at least 2×10^4 in order to ensure the independence of internal flow on the Reynolds number. However, it should be noted that the velocity at the average height of the opening differs by a factor of ≈2 between two modelled ABLs (see Fig. 2a), which will be discussed in due course.

2.2. Measurement and data-processing techniques

A 2D time-resolved particle image velocimetry (TR-PIV) system from Dantec Dynamics was used at a repetition rate of 200 Hz to capture the time evolution of the flow within the model of the cattle barn. The laser sheet from DualPower 30–100 laser was positioned vertically nearby the middle of the openings (75 mm laterally from the centre of the model, see Fig. 1a) to light particles carried by the flow within the barn at that plane. A Laskin nozzle generator upstream of the vortex generators continuously injected the particles (about 1 μm in diameter) to the flow. The CMOS camera SpeedSense VEO 410 captured 6227 consecutive double-frames during an acquisition time of 30 s for each studied case and plane. Such acquisition time provides robust velocity time series to perform statistically independent analysis as well. The instantaneous velocity vector fields were computed using Adaptive PIV method by DynamicStudio software. The size of the interrogation area was set to 32 × 32 pixels with 50% overlap, which resulted in 5 mm (0.026H) of the spatial resolution of the velocity vector field. The relative measurement error of the mean velocities and turbulent kinetic energy (TKE) was estimated from the four TR-PIV runs performed for the case R4-O (that means for the rural ABL, quarter open sidewall openings, doors open and without cows) not be higher than 2.5% and 7.2%, respectively.

A fast flame ionisation detector (FFID) from Cambustion Ltd performed point concentration measurements of ethane within the model of cattle barn at a repetition rate about 200 Hz. A unique 400 mm long sampling tube was designed to measure the ethane concentrations close to the cattle barn bottom, without interrupting the flow around the model. The tube was positioned into the barn model through the holes (4 mm in diameter) along the centreline in the roof utilising a three-dimensional traverse system (Fig. 1b). The FFID sampling points were distributed evenly within the vertical plane. This plane was positioned 12 mm closer to the centre of the model (y = −63, see Fig. 1b) than the plane for the PIV measurements and at the centre of the openings. Each of the measurements (the flow and the concentration) was performed separately. During concentration measurements through a given hole, the other holes were sealed. The relative error (4%) of the concentration measurements was estimated from 40 runs performed for four (10 runs for each) different sampling positions within the cattle barn model. A dimensionless concentration, $C^* = CU_{ref}A/Q$, where C is the measured concentration in ppm, A is the total pollution source area in m^2, and Q is the ethane flow rate from the source in m^3 s^{-1} was used to compare the studied cases.

3. Results and discussions

3.1. The mean flow field

Fig. 3 demonstrates a clear impact of the sidewall openings and ABL on the mean flow (time-averaged streamlines) field within the model of the cattle barn. The dimensionless resulting 2D velocity (computed as $(U^2+W^2)^{0.5}/U_{ref}$, where U and W is the mean streamwise and vertical velocity, respectively) coloured the streamlines. All cases presented Fig. 3 have open doors and no cows in the barn.

The fully open configuration (Fig. 3a) enables the outdoor wind to blow with ease through the barn to the outlet opening in the case of the rural ABL. This blow produces a jet at the lower part and an anticlockwise-rotating vortex at the upper part of the barn. A quantitative comparison between the vertical profiles of the mean dimensionless streamwise velocity ($U/U_{h,}$ where U_h is the mean wind speed at the building height obtained from the measured ABL velocity profiles during the absence of the model) from the present study and those from the study of Shen et al. (2016) and Yi et al. (2018a), both using a laser Doppler anemometry (LDA), is presented in Fig. 2d. Shen et al. (2016) observed the similar flow patterns, although their model of the barn did not have the ridge and doors openings. Interestingly, the profiles presented for Yi et al. (2018) do not confirm the flow patterns observed

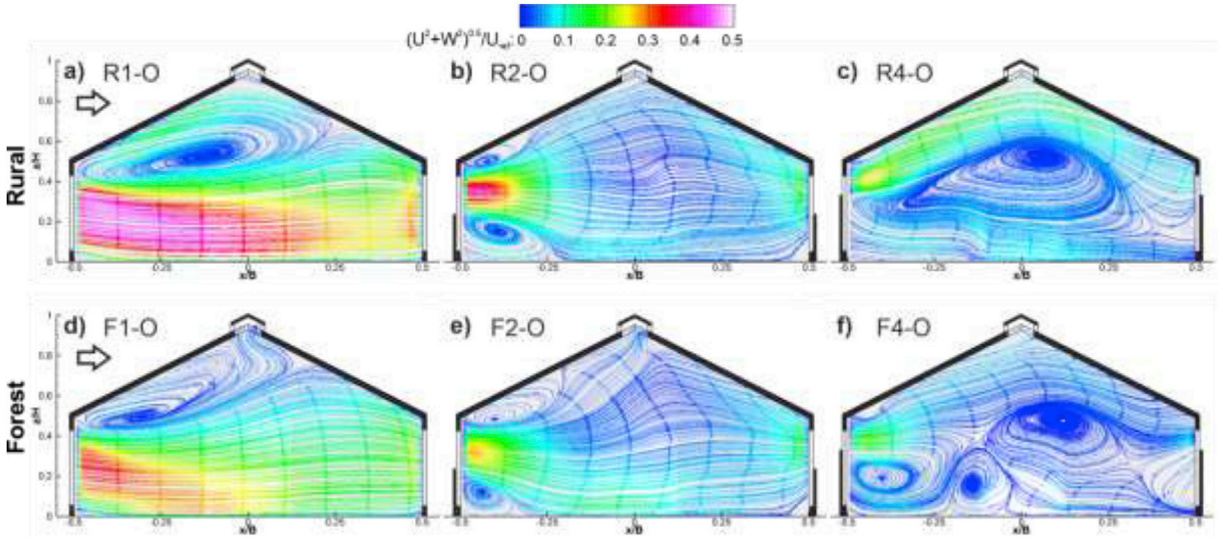

Fig. 3. Mean 2D streamlines at the vertical planes for the (**a,d**) full, (**b,e**) half, and (**c,f**) quarter open openings and the (**a-c**) rural and (**d-f**) forest approach boundary layers. In all cases, the doors are open, and there are no cows. The streamlines are coloured by the dimensionless resultant (2D) velocity. The arrow at the top left represents the direction of the approaching wind.

either our or Shen et al. (2016) study. The main explanations might be twofold. First, the different ridge opening geometry (formed only by one opening at the leeward side of the barn roof compared to the symmetrical openings at both sides in the present study) used by Yi et al. (2018a) drains off the flow below the roof more than in our case or in the case of Shen et al. (2016), and hence likely destroy the anticlockwise-rotating vortex at the upper part of the barn. Secondly, the approaching ABL simulated in our case differs (primarily in the friction velocity and spectrum of turbulence) from that simulated by Yi et al. (2018a) in their wind tunnel. However, the turbulent kinetic energy (TKE) has similar distribution within the barn as in our case (Fig. 2e).

In the case of the half-open configuration (Fig. 3b), the anticlockwise vortex is suppressed close to the inlet, and a new, smaller, clockwise vortex is generated just downwind the sidewall. These two vortices are the result of the shear layers produced at the upper and lower edge of the incoming jet. For the quarterly open case (Fig. 3c), the incoming flow attaches to the roof, and the well-known Coanda effect can be observed due to the higher static pressure (lower flow velocity) in the middle of the

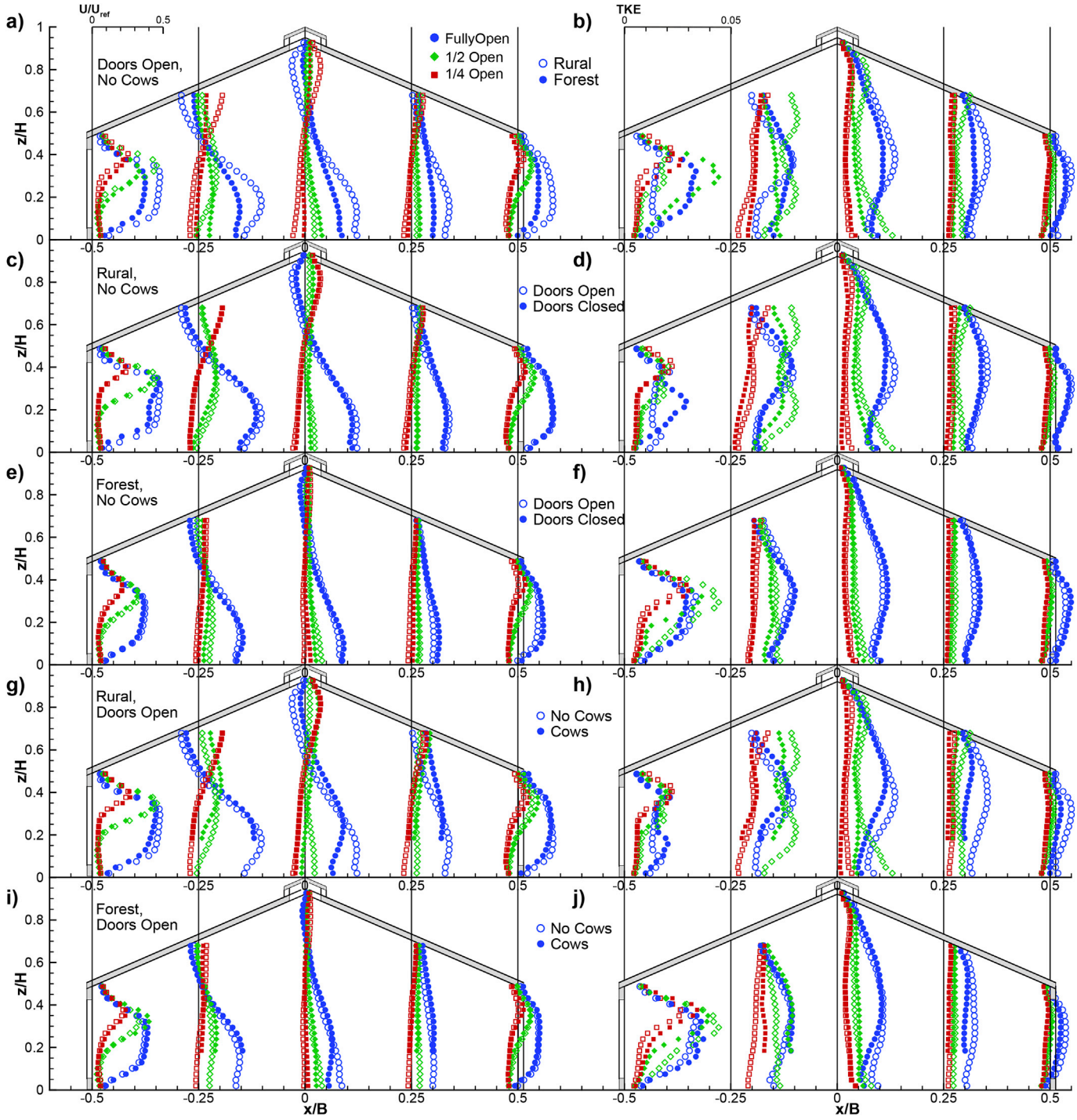

Fig. 4. Vertical profiles of the mean dimensionless longitudinal velocity (**a,c,e,g,i**) and 2D turbulent kinetic energy (**b,d,f,h,j**) at five streamwise positions ($x/B = -0.48, -0.25, 0, 0.25$ and 0.48) of the measured vertical plane. (**a,b**) the impact of the simulated ABL; (**c-f**) the impact of the doors; (**g-j**) the impact of the cows. The *circles*, *diamonds* and *squares* are for the full, half and quarter openings' configurations, respectively. Note that the relative error bars are not presented due to their size smaller than symbols.

barn. Such a flow attachment was also reported by Morsing et al. (2002) for the similar opening geometry and the cattle barn model, and also by Tominaga and Blocken (2016) for a model of a generic building. Downstream, the flow falls to the model bottom and reverses back to the inlet wall, producing a weak anticlockwise vortex at the centre of the barn.

The change of ABL from a moderately (e.g., induced by a rural terrain) to very rough (e.g., induced by forest) also produced appreciable changes in flow patterns within the barn. A weaker (by a factor of ≈2) but more turbulent wind impacts the opening in the case of the forest ABL which in turn produces weaker blows into the barn and weaker and smaller vortices within the barn in all cases of opening configurations (Fig. 3d–f). These findings support those reported by Ramponi and Blocken (2012) who in their CFD study on a generic building show that the turbulence in the approaching flow strongly influences the flow indoors. Specifically, they found that the increase of the physical and numerical diffusion in the flow approaching the building increases the spread of the jet entering the buildings.

To compare all the studied cases quantitatively, the vertical profiles of the mean dimensionless streamwise velocity and two-dimensional TKE extracted from five streamwise positions (x/B = −0.48, −0.25, 0, 0.25 and 0.48) within the barn are compared in Fig. 4. It should be noted that TKE was computed as $0.75(\sigma_U^2 + \sigma_W^2)$, where σ_U and σ_W are the standard deviations of the streamwise and vertical velocity, respectively, by the DynamicStudio software to approximate a 3D TKE. Again apparent effects of the sidewall opening and ABL on the mean flow (Fig. 4a) but also the turbulence (Fig. 4b) can be seen, although the ABL has a less significant impact on the flow in the cases of smaller openings (half and quarter) further downstream ($x/H > 0.25$) within the barn. The rural ABL produces appreciably higher velocities in case of the fully (empty blue circles in Fig. 4a) and the quarter (meaning also the negative velocities, see empty red squares in Fig. 4a) open configuration. However, in the case of the half-open width and up to the first half of the barn ($-0.5 < x/B < 0$), the forest ABL (green filled diamonds in Fig. 4a) drives faster flow nearby the bottom ($z/H < 0.25$) than the rural ABL (empty green diamonds in Fig. 4a). A similar effect might be observed for the TKE, but all studied openings (Fig. 4b).

The impact of doors opening on the mean flow near the middle of the barn is negligible when the wind is perpendicular to sidewalls (Fig. 4c and e) but has some effect on turbulence (Fig. 4d and f). Generally, the TKE decreases if the doors are closed irrespective of the studied ABL. Similar conclusions might be drawn in case of the presence of cows (Fig. 4g–j). Indeed, there is a notable difference between the mean flow produced by the cows and that produced by their absence in the middle of the barn, but in other areas, there are no appreciable changes between these two flows. Interestingly, the turbulence is damped by the cows further downstream within the barn in the case of fully open configuration (compare blue empty and filled circles in Fig. 4h and j). It should be noted that no heat production of cows has been simulated and that only the wind perpendicular to the sidewall openings was performed. These two parameters (the heat production and the wind direction) might have a significant impact on studied airflow patterns within a barn and hence are worthy of further investigation.

3.2. Flow structures stability analysis

In turbulence research, it is well known that despite the chaotic nature of turbulence organised structures – *coherent structures* – might be observed in the flow. These structures are essential for transport processes as has been demonstrated by previous studies (Conan et al., 2015; Luo et al., 2012; Nosek et al., 2017; Raupach et al., 1996). Since the time-resolved data from PIV measurements are obtained in this study, the oscillation pattern decomposition (OPD) method provided by Dantec-Dynamics software is used to identify the dynamics and topology of these structures. Mainly, the OPD method enables to reveal the "hidden" coherent structures of the flow, which are the most stable (lasting the longest in the flow). Compared to widely-used Proper Orthogonal Decomposition (POD) (e.g., Berkooz et al., 1993) or Bi-Orthogonal Decomposition (BOD) method (e.g., Aubry, 1991), OPD provides information about the frequency at which the structures are excited into the flow and how they propagate in the space.

The OPD method is based on Principal Oscillation Patterns (POP) introduced by Hasselmann (1988) and Von Storch et al. (1988) in climatology and is similar to another well-known Dynamic Mode Decomposition (DMD) method introduced by Schmid (2010). The POP is the linearised form of the more general Principal Interaction Pattern (PIP) method, which constructs simplified dynamical models to approximate complex nonlinear systems with many degrees of freedom (Hasselmann, 1988). The starting point of both the OPD and DMD is that the fluctuating part of Navier–Stokes equation is modelled by Langevin equation for the linear Markov process, but for the OPD method the eigenmodes of the deterministic feedback matrix of Langevin equation is evaluated differently (Uruba, 2015). However, both OPD and DMD methods provide complex eigenvalues and eigenvectors. While the complex eigenvectors reveal the structure (OPD mode) topology and how this structure propagate in space, the complex eigenvalue defines the frequency (f), at which the structure was excited into the flow and time, so-called e-fold time (t_e), at which the amplitude of the structure's oscillation decays to $1/e$. The most stable dynamic structures decomposed from the instantaneous flow filed are those which have the highest periodicity, $p = f.\ t_e$. Indeed, the e-fold time is the crucial parameter here, but if there is no oscillation ($f = 0$), there is no dynamics, and hence the e-fold time characterises a pulsating structure without any propagation in space (Von Storch et al., 1988). Uruba (2015) proposed the threshold value of $p = 0.43$, which means that bellow this value the structure's amplitude decays faster than by factor 10 during the period, and hence a non-oscillating rapidly decaying mode (structure) is detected in the flow.

To save the computational time, DynamicStudio software computes the OPD eigenvectors and eigenvalues from the already computed "topos" and "chronos" from POD analysis. Therefore, the first POD modes are presented as well, which represent those structures having the highest contribution (E_r) to the total turbulent kinetic energy of the flow field and compare them with those from the OPD analysis. It should be noted that the POD modes contain a broad mix of different frequencies without any information on their phase and hence represent non-dynamic structures. The OPD analysis was set to compute all the POD modes, which have $E_r > 0.005$.

Fig. 5 compares topology (complex eigenvectors) of the most stable OPD modes (the first and second column in Fig. 5) and the most energetic POD modes (the third column in Fig. 5) concerning the opening width and modelled ABL. Here, the most stable OPD mode represents the mode that has the highest periodicity, p. The propagation of the OPD modes is demonstrated through their phases (ϕ), and only the two phases, $\phi = 0$ and 90°, which correspond to the real and imaginary part of the eigenvectors, respectively, is presented in Fig. 5 for clarity. The coloured contours in Fig. 5 represent the vorticity, while the streamlines represent the topology of the vortical structures. The speed of the structure propagation was estimated as $U_c = f.s$, where s is the structure spacing (Fig. 5a).

From the first glance of view, one can observe the absolute difference in topology between the POD and OPD modes. The most energetic structures form one (third column in Fig. 5a and b) or maximum of two (third column in Fig. 5c–f) vortices, while the most stable dynamic structures manifest the Kelvin-Helmholtz instability of the flow producing the several vortices propagating through the barn (first and second column in Fig. 5). A similar instability was qualitatively observed by Tominaga and Blocken (2015) during visualisation tests for a naturally ventilated generic building. The most stable dynamic structures have at least three vortices and are more dependent on the studied case (Fig. 5). They propagate from the inlet opening to the outlet, but only in the case of the fully open configuration the vortices are also presented at the outlet opening, thus do not vanish within the remaining part of the barn

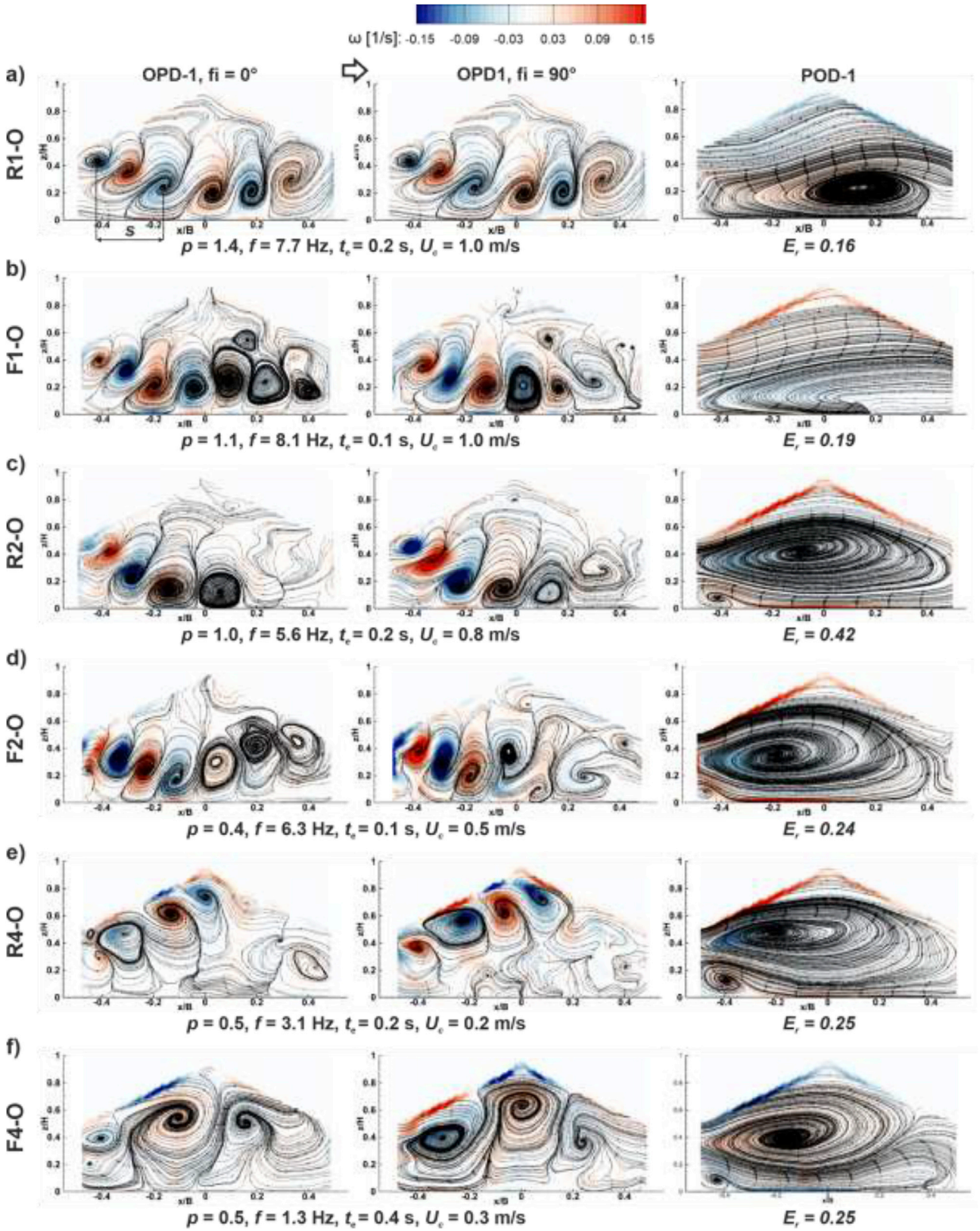

Fig. 5. Cyclic propagation (i.e. $\phi = 0°$ and 90°) of the most periodical (stable) OPD modes through the cattle barn in case of the rural (**a,c,e**) and forest (**b,d,f**) ABL and in cases of the fully (**a,b**), half (**c,d**) and quarter (**e,f**) open openings. The first column represents the real part ($\phi = 0°$), while the second column the imaginary part ($\phi = 90°$) of the OPD modes. The topology of those structures having the highest contribution to the total TKE (the first POD modes) is presented in the third column for the comparison. The contours represent the vorticity of the structures. The structures' spacing is denoted by s from which the convective velocity of the OPD structures, U_c, was computed.

as in the other cases. Irrespective of the studied case, the periodicity (p) and the speed of structures propagation (U_c) decrease with the decrease of the opening size. The smaller opening damps the frequency at which the structures are excited into the flow. Due to the lower frequency, the larger structures occur, and hence their spacing which propagates slower. The angle (about −30°) of the direction of propagation is the same for both the full (Fig. 5a and 5b) and the half (Fig. 5c and 5d) opening but changes about 60° (to approx. 30°) in the case of the quarter opening (Fig. 5e and 5f). One can also observe the impact of ABL on the topology of dynamic structures from the two phases (0° and 90°) presented in Fig. 5, and that the less turbulent ABL (Fig. 5a, c, and e) produces more stable (with higher periodicity) dynamic structures than the more turbulent approaching ABL.

3.3. The pollutant dispersion within the barn

From the mean concentration fields and vertical profiles presented in Figs. 6 and 7, respectively, one can see that the type of the opening configuration and the type of simulated ABL have an appreciable impact on the cattle barn ventilation. Indeed, the lower the opening width, the higher concentration levels are within the entire barn. The rural ABL produces lower concentration levels (Fig. 6a, c, and e) at some areas compared to the forest ABL (Fig. 6b, d, and f) due to the higher and more uniform flow impacting the inlet openings which result in higher internal flows. The position of both the planar source and the openings has a crucial impact on the concentration distribution. While one can find the lowest concentrations nearby the inlets, the highest concentration levels are at the bottom and in the regions where the mean vortices dominate (manifested by the velocity vectors in Fig. 6c–f). From Fig. 6 can also be observed a downstream and upstream advection of the pollutant according to the mean flow and spatial distribution of the concentration as the concentrations increase downstream in the fully open case (Fig. 6a) and upstream in the quarter open case (Fig. 6e), respectively. The highest polluted spots correspond to the areas where the flow is stagnant, and hence of poor pollutant transport (see, e.g., the lower downstream corner in Fig. 6f). The pollutant transport can be hardly observed from the mean vertical concentration lines presented in Fig. 7. However, these lines give a better quantitative comparison among studied cases.

In terms of the concentration diffusion, the mean concentration fluctuations (e.g., Fig. 7b) follow the mean concentration gradients (Fig. 7a) instead of the mean velocity fluctuations (Fig. 4b). The same was observed by Tominaga and Blocken (2015), and hence confirms their suggestion that different mechanisms drive each of the fluctuations separately. However, since one can observe a spatial correlation between the spatial distribution of the mean concentration and the topology and direction of the propagation of the most stable dynamic coherent structures (compare Figs. 5 and 6), these structures seem to play another role for pollutant dispersion within the barn.

The presence of cows has a negligible impact on the pollutant dispersion within the barn (see Fig. 7b–c) as having been already

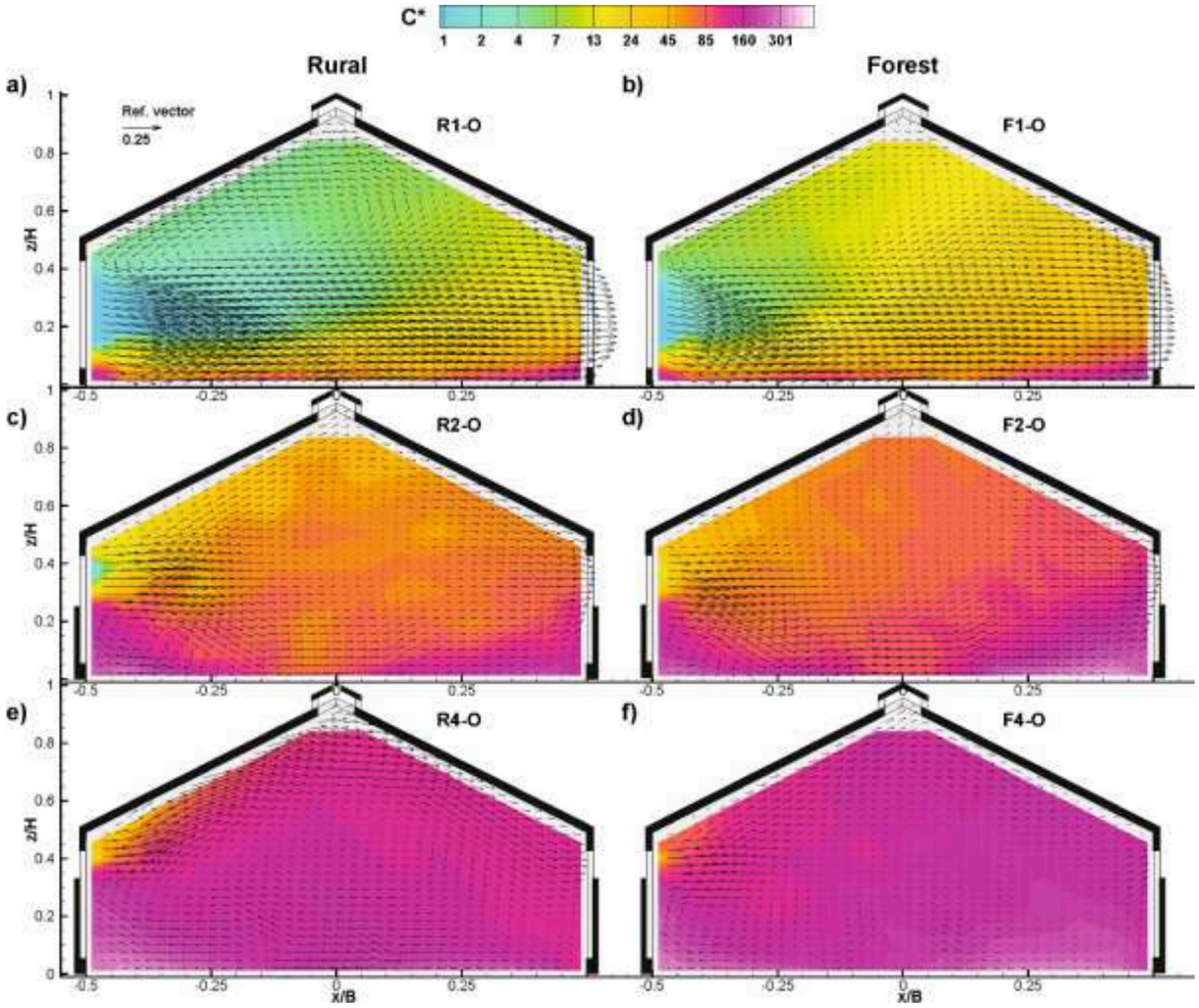

Fig. 6. Mean dimensionless concentration (contours) and flow fields (vectors (u,w)) at the vertical plane for the (**a,b**) full, (**c,d**) half, and (**e,f**) quarter openings configurations and the (**a,c,e**) rural and (**b,d,f**) forest approach boundary layers. Every second velocity vector (u,w) is plotted for the sake of clarity.

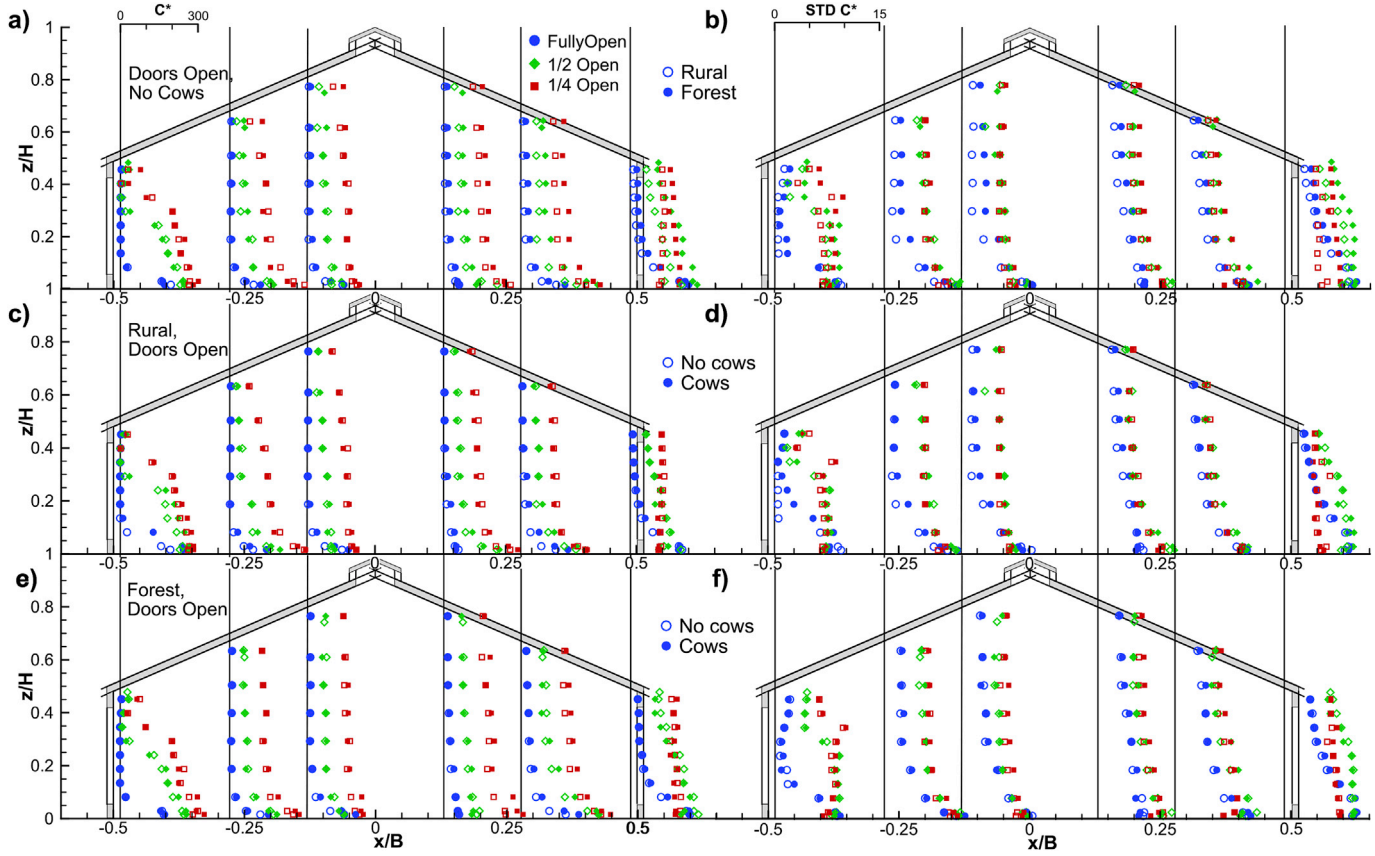

Fig. 7. Vertical profiles of the mean (**a,c,e**) and standard deviation (**b,d,f**) of dimensionless concentration at six streamwise positions ($x/B = -0.48$, -0.28, -0.13, 0.13, 0,28 and 0.48) of the measured vertical plane. (**a,b**) the impact of the simulated ABL; (**c-f**) the impact of the cows. The *circles*, *diamonds* and *squares* are for the full, half and quarter openings' configurations, respectively. Note that the relative error bars are not presented due to their size smaller than symbols.

observed during the mean flow and TKE analysis (Fig. 4c–f), and analysis of the coherent structures (not shown here). However, there is one exception, and that is the fully open configuration simulated for the rural ABL (Fig. 7d).

3.4. Ventilation performance – comparison of different methods

Fig. 6 clearly shows that the pollutant within the barn is not well mixed in any case. Such imperfect mixing reflects the flow field characteristics within the barn and the position of the source. A spatially averaged (plane-averaged, in our case) concentration provides additional information about the ventilation performance of the cattle barn. In most cases (especially in-situ), the spatial distribution of pollutant concentration is not known a priori, and other methods such as tracer gas method or air exchange rate index are widely used to evaluate the ventilation performance. However, such methods are based on the assumption that the pollutant is well mixed within the barn. Therefore, a one-point- and line-averaged concentration and ventilation rate is compared with the plane-averaged concentration (C^*_{pl}) to observe possible underestimation/overestimation of the cattle barn ventilation performance estimated by these parameters.

The mean dimensionless concentration in middle of the barn (x/B = 0, z/H = 0.4) was used for the one-point-averaged concentration (C^*_p), while the line-averaged concentration (C^*_{lin}) was computed as

$$C^*_{lin} = \frac{1}{D}\int_{-D/2}^{D/2} C^* dz, \tag{1}$$

at the outlet opening (x/B = 0.45). The dimensionless ventilation rate (Q) was computed at the inlet opening (x/B = −0.45) as

$$Q = \frac{1}{DU_{ref}}\int_{-D/2}^{D/2} U dz, \tag{2}$$

where D is the opening height and U is the mean streamwise velocity at the given point. The relative plane-averaged concentration ($C^*_{pl,rel}$) and relative ventilation rate (Q_{rel}) were normalised by the plane-averaged concentration and ventilation rate in the case of R1-O, respectively, to generalise the results.

Fig. 8a shows that the plane-averaged concentration is in line with what was previously observed during the flow and pollutant dispersion analysis: the opening configuration and the type of ABL have a significant impact on the cattle barn ventilation. Fig. 8a also demonstrates that fully open cases are about 5 and 10 times more ventilated than the half and quarter open configurations, respectively. However, if one uses the line (Fig. 8b) or one-point-averaged (Fig. 8c) concentration, a significant underestimation (up to by a factor of 3) of the ventilation performance might achieve. Both these concentrations reach the plane-averaged concentration level in the case of the quarter open configuration. This indicates that the concertation within the barn is more evenly distributed during the quarter open case than in the other cases.

Concerning the ventilation rate, similar results are obtained in the estimation of the barn ventilation performance (Fig. 8d). However, the ventilation rate underestimates the barn ventilation more significantly (by a factor of 5) compared to the plane-averaged concentration levels (e.g. $C^*_{pl,rel}$ is almost 12 times higher in the case of F4–O than R1-O, while Q_{rel} predicts the ventilation about 2.5 times lower considering the same case comparison). This is primarily brought about by the difference of flow patterns observed inside the barn for different opening heights and simulated ABL, and by the source characteristics (its type and position). These main mechanisms of the pollutant dispersion inside the barn cannot be captured by the flow characteristics measured at the openings,

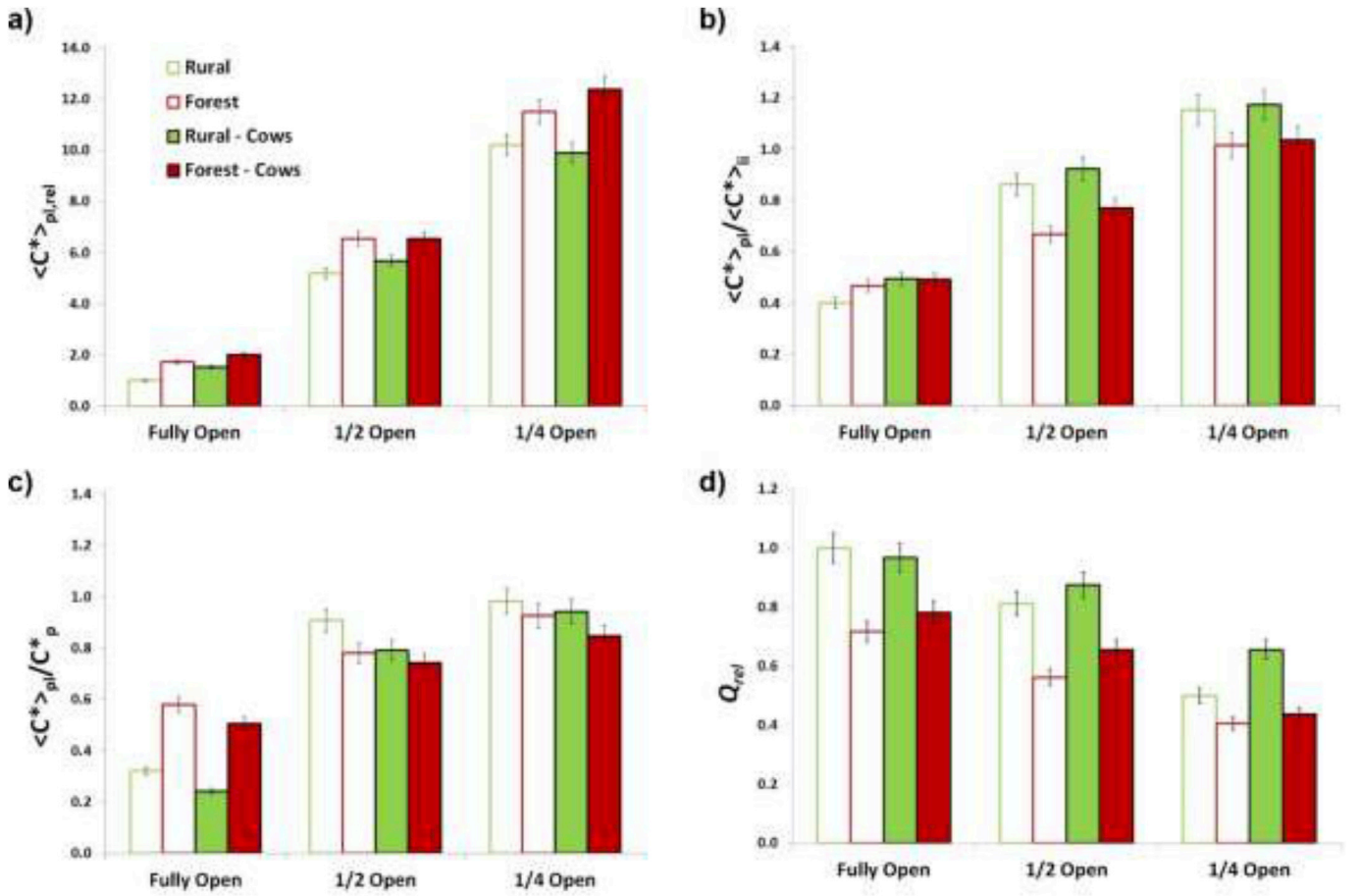

Fig. 8. (**a**) Relative plane-averaged concentration ($<C^*>_{pl,rel}$); (**b**) ratio of the plane-averaged concentration to the line-averaged concentration at the outlet opening ($<C^*>_{pl}/(<C^*>_{lin}$); (**c**) ratio of the plane-averaged concentration to the point-averaged concentration in the middle of the barn ($<C^*>_{pl}/(<C^*>_{p}$); (**d**) the relative ventilation rate (Q_{rel}).

and hence the ventilation rate underestimates the barn ventilation. A similar inconsistency between the ventilation performance parameters was observed by Tominaga and Blocken, 2016 for a generic building and highlight that care should be applied when evaluating ventilation performance from flow rates or concentration values measured at one point only. Such caution is also confirmed by the present study for naturally ventilated livestock buildings, where the source of pollution is mostly planar, and the flow characteristics captured just at the openings cannot predict the ventilation of the barn accurately.

4. Conclusions

This paper brings a new and detailed insight into dispersion processes in a naturally ventilated livestock building. The impact of the atmospheric boundary layer (ABL), type of openings and presence of animals on the flow and pollutant dispersion in a model of cattle barn was studied under controlled conditions in a wind tunnel with perpendicular wind conditions. It was demonstrated that the ventilation opening width and the type of ABL have a crucial impact on both the flow and pollutant dispersion within the barn, while the presence of cows (without heat production) and doors openings are insignificant. However, this might not be true if the wind is not perpendicular to the ventilation openings or the heat production of cows are take into account. Another limitation is that 3D effects (the 2D velocities and concentrations were investigated only at one vertical plane) were not addressed in the present study. Therefore, further studies are needed to clarify the effect of these parameters on flow and pollutant dispersion within a cattle barn.

It was found that the indoor cattle barn pollution levels decrease proportionally with the increase of the ventilation opening width. A similar proportionality was found in terms of the simulated ABL. When the cattle barn is exposed to a more rough ABL (e.g., forest or hilly terrain), a significant increase of pollutant concentration within the barn was observed in comparison to a less rough ABL (e.g. rural terrain). This is due to the weaker and less uniform flow impacting the openings in the case of the more rough ABL, which in turn produces slower and less turbulent internal flows compared to the less rough ABL. These findings were demonstrated not only on the mean flow patterns but also on dynamics of coherent structures developed within the barn using time-resolved PIV technique and Oscillating Pattern Decomposition (OPD) method. The dynamic structures manifest the well-known Kelvin-Helmholtz instability in every studied case, and, unlike non-dynamic (but the most energetic) coherent structures, they spatially correlate with the mean concentration fields and concentration fluctuations. Irrespective of the studied case, the stability and the speed of structures propagation decreased with the decrease of the opening size. The smaller opening damps the frequency at which the structures are excited into the flow. Due to the lower frequency, the larger structures occur, and hence their spacing which propagates slower. These findings show that the dynamic coherent structures play another important role in the pollutant transport within the barn.

The findings of Tominaga and Blocken, 2015, who observed for a cross-ventilated generic building that fluctuations of velocity are driven by the shear layers of the flow, while the mean concentration gradients drive fluctuations of concentration, were confirmed by the present study. The present study also confirms that in any of the studied cases the pollutant was not well-mixed within the building, and hence significant underestimation or overestimation (up to by factor 5) of the building ventilation might be obtained using, e.g. tracer gas method.

Declaration of competing interest

The authors declare that they have no known competing financial interests or personal relationships that could have appeared to influence the work reported in this paper.

CRediT authorship contribution statement

Štěpán Nosek: Conceptualization, Methodology, Investigation, Writing - original draft. **Zuzana Kluková:** Investigation, Data curation. **Michala Jakubcová:** Software, Visualization. **Qianying Yi:** Writing - review & editing. **David Janke:** Writing - review & editing, Validation. **Peter Demeyer:** Validation. **Zbyněk Jaňour:** Conceptualization, Supervision.

Acknowledgement

The authors gratefully acknowledge funding from the Ministry of Education, Youth and Sports of CR (LTC18070) and from the institutional support RVO:61388998. Further this article is based upon cooperation from COST Action LivAGE (CA16106), supported by COST (European Cooperation in Science and Technology). Authors also would like to thank prof. Vaclav Uruba for his consultations to OPD analysis, and Dr. Pavel Procházka and Jan Kozohorský for their valuable support during the experiments.

References

Arogo, J., Zhang, R.H., Riskowski, G.L., Day, D.L., 1999. Mass transfer coefficient for hydrogen sulfide emission from aqueous solutions and liquid swine manure. Trans. ASABE (Am. Soc. Agric. Biol. Eng.) 42, 1455–1462.

Aubry, N., 1991. On the hidden beauty of the proper orthogonal decomposition. Theor. Comput. Fluid Dynam. 2, 339–352. https://doi.org/10.1007/BF00271473.

Berkooz, G., Holmes, P., Lumley, J.L., 1993. The proper orthogonal decomposition in the analysis of turbulent flows. Annu. Rev. Fluid Mech. 25, 539–575.

Bjerg, B., Norton, T., Banhazi, T., Zhang, G., Bartzanas, T., Liberati, P., Cascone, G., Lee, I., Marucci, A., 2013. Review Modelling of ammonia emissions from naturally ventilated livestock buildings. Part 1 : ammonia release modelling. Biosyst. Eng. 116, 232–245. https://doi.org/10.1016/j.biosystemseng.2013.08.001.

Cermak, J.E., Poreh, M., Peterka, J.A., Ayad, S.S., 1984. Wind tunnel investigations of natural ventilation. J. Transport. Eng. 110, 67–79. https://doi.org/10.1061/(ASCE)0733-947X, 1984)110:1(67.

Choiniere, Y., Blais, F., Munroe, J., 1988. A wind tunnel study of airflow patterns in a naturally ventilated building. Can. Agric. Eng. 293–297.

Conan, B., Aubrun, S., Coudour, B., Chetehouna, K., Garo, J.-P., 2015. Contribution of coherent structures to momentum and concentration fluxes over a flat vegetation canopy modelled in a wind tunnel. Atmos. Environ. 107, 329–341. https://doi.org/10.1016/j.atmosenv.2015.02.061.

Counihan, J., 1975. Adiabatic atmospheric boundary layers: a review and analysis of data from the period 1880–1972. Atmos. Environ. 9, 871–905. https://doi.org/10.1016/0004-6981(75)90088-8.

De Paepe, M., Pieters, J.G., Cornelis, W.M., Gabriels, D., Merci, B., Demeyer, P., 2013. Airflow measurements in and around scale-model cattle barns in a wind tunnel: effect of wind incidence angle. Biosyst. Eng. 115, 211–219. https://doi.org/10.1016/j.biosystemseng.2013.03.008.

De Paepe, M., Pieters, J.G., Mendes, L.B., Van Weyenberg, S., Merci, B., Demeyer, P., 2016. Wind tunnel study of ammonia transfer from a manure pit fitted with a dairy cattle slatted floor. Environ. Technol. (United Kingdom) 37, 202–215. https://doi.org/10.1080/09593330.2015.1066449.

Fiedler, M., Schröter, K., Reinhardt, A., Saha, C., Loebsin, C., Berg, W., Amon, T., 2013. Wind tunnel investigations on a naturally ventilated barn. Landtechnik 68, 265–268.

Hasselmann, K., 1988. PIPs and POPs: the reduction of complex dynamical systems using principal interaction and oscillation patterns. J. Geophys. Res. 93, 11015–11021. https://doi.org/10.1029/JD093iD09p11015.

Ikeguchi, A., Okushima, L., Zhang, G., Strom, J.S., 2005. Contaminant air propagation between naturally ventilated scale model pig buildings under steady-state conditions. Biosyst. Eng. 90, 217–226. https://doi.org/10.1016/j.biosystemseng.2004.10.011.

Ikeguchi, A., Zhang, G., Okushima, L., Bennetsen, J.C., 2003. Windward windbreak effects on airflow in and around a scale model of a naturally ventilated pig barn. Trans. ASAE 46. https://elibrary.asabe.org/azdez.asp?AID=13594&T=2, 789-795.

Krupa, S.V., 2003. Effects of Atmospheric Ammonia (NH 3) on Terrestrial Vegetation : a Review, vol. 124, pp. 179–221. https://doi.org/10.1016/S0269-7491(02)00434-7.

Luo, J.P., Lu, Z.M., Qiu, X., Li, D.M., Liu, Y.L., 2012. Effect of sweep and ejection events on particle dispersion in wall bounded turbulent flows. J. Hydrodyn. 24, 794–799. https://doi.org/10.1016/S1001-6058(11)60305-3.

Meroney, R.N., Pavageau, M., Rafailidis, S., Schatzmann, M., 1996. Study of line source characteristics for 2-D physical modelling of pollutant dispersion in street canyons. J. Wind Eng. Ind. Aerod. 62, 37–56.

Morsing, S., Ikeguchi, A., Bennetsen, J.C., Strøm, J.S., Ravn, P., Okushima, L., 2002. Wind induced isothermal airflow patterns in a scale model of a naturally ventilated swine barn with cathedral ceiling. Appl. Eng. Agric. 18, 97–101.

Norton, T., Grant, J., Fallon, R., Sun, D.W., 2009. Assessing the ventilation effectiveness of naturally ventilated livestock buildings under wind dominated conditions using computational fluid dynamics. Biosyst. Eng. 103, 78–99. https://doi.org/10.1016/j.biosystemseng.2009.02.007.

Nosek, Š., Kukačka, L., Jurčáková, K., Kellnerová, R., Jaňour, Z., 2017. Impact of roof height non-uniformity on pollutant transport between a street canyon and intersections. Environ. Pollut. 227, 125–138. https://doi.org/10.1016/j.envpol.2017.03.073.

Olesen, J., Sommer, S., 1993. Modeling effects of wind-speed and surface cover on ammonia volatilization from stored pig slurry. Atmos. Environ. Part a-General Top. 27, 2567–2574. https://doi.org/10.1016/0960-1686(93)90030-3.

Ramponi, R., Blocken, B., 2012. CFD simulation of cross-ventilation flow for different isolated building configurations: validation with wind tunnel measurements and analysis of physical and numerical diffusion effects. Jnl. Wind Eng. Ind. Aerodyn. 104– 106, 408–418. https://doi.org/10.1016/j.jweia.2012.02.005.

Raupach, M.R., Finnigan, J.J., Brunei, Y., 1996. Coherent eddies and turbulence in vegetation canopies: the mixing-layer analogy. Boundary-Layer Meteorol. 78, 351–382. https://doi.org/10.1007/BF00120941.

Rong, L., Bjerg, B., Zhang, G., 2015. Assessment of modeling slatted floor as porous medium for prediction of ammonia emissions - scaled pig barns. Comput. Electron. Agric. 117, 234–244. https://doi.org/10.1016/j.compag.2015.08.007.

Rong, L., Nielsen, P.V., Zhang, G., 2009. Effects of airflow and liquid temperature on ammonia mass transfer above an emission surface: experimental study on emission rate. Bioresour. Technol. 100, 4654–4661. https://doi.org/10.1016/j.biortech.2009.05.003.

Schatzmann, M., Leitl, B., 2011. Issues with validation of urban flow and dispersion CFD models. J. Wind Eng. Ind. 99, 169–186. https://doi.org/10.1016/j.jweia.2011.01.005.

Schatzmann, M., Olesen, H., Franke, J., 2010. COST 732 Model Evaluation Case Studies: Approach and Results (Hamburg).

Schmid, P., 2010. Dynamic mode decomposition of numerical and experimental data. J. Fluid Mech. 656, 5–28. https://doi.org/10.1017/S0022112010001217.

Shen, X., Su, R., Ntinas, G.K., Zhang, G., 2016. Influence of sidewall openings on air change rate and airflow conditions inside and outside low-rise naturally ventilated buildings. Energy Build. 130, 453–464. https://doi.org/10.1016/j.enbuild.2016.08.056.

Shen, X., Zhang, G., Bjerg, B., 2013. Assessments of experimental designs in response surface modelling process: estimating ventilation rate in naturally ventilated livestock buildings. Energy Build. 62, 570–580. https://doi.org/10.1016/j.enbuild.2013.03.038.

Tominaga, Y., Blocken, B., 2016. Wind tunnel analysis of flow and dispersion in cross-ventilated isolated buildings: impact of opening positions. Jnl. Wind Eng. Ind. Aerodyn. 155, 74–88. https://doi.org/10.1016/j.jweia.2016.05.007.

Snyder, W., 1981. Guideline For Fluid Modeling Of Atmospheric Diffusion. EPA.

Tominaga, Y., Blocken, B., 2015. Wind tunnel experiments on cross-ventilation fl ow of a generic building with contaminant dispersion in unsheltered and sheltered conditions. Build. Environ. 92, 452–461. https://doi.org/10.1016/j.buildenv.2015.05.026.

Uruba, V., 2015. Near wake dynamics around a vibrating airfoil by means of PIV and Oscillation Pattern Decomposition at Reynolds number. J. Fluid Struct. 55, 372–383. https://doi.org/10.1016/j.jfluidstructs.2015.03.011.

Vdi Verein Deutcher Ingenieure, 2000. Physical Modelling of Flow and Dispersion Processes in the Atmospheric Boundary Layer - Application of Wind Tunnels. VDI Verein Deutcher Ingenieure, Düsseldorf.

Von Storch, H., Bruns, T., Fischer-Bruns, I., Hasselmann, K., 1988. Principal oscillation pattern analysis of the 30- to 60-day oscillation in general circulation model equatorial troposphere. J. Geophys. Res. 93, 22–36. https://doi.org/10.1029/JD093iD09p11022.

Wu, W., Zhai, J., Zhang, G., Nielsen, P.V., 2012. Evaluation of methods for determining air exchange rate in a naturally ventilated dairy cattle building with large openings using computational fluid dynamics (CFD). Atmos. Environ. 63, 179–188. https://doi.org/10.1016/j.atmosenv.2012.09.042.

Yi, Q., König, M., Janke, D., Hempel, S., Zhang, G., Amon, B., Amon, T., 2018a. Wind tunnel investigations of sidewall opening effects on indoor airflows of a cross-ventilated dairy building. Energy Build. 175, 163–172. https://doi.org/10.1016/j.enbuild.2018.07.026.

Yi, Q., Wang, X., Zhang, G., Li, H., Janke, D., Amon, T., 2019. Assessing effcts of wind speed and wind direction on discharge coefficient of sidewall opening in a dairy building model – a numerical study. Comput. Electron. Agric. 162, 235–245. https://doi.org/10.1016/j.compag.2019.04.016.

Yi, Q., Zhang, G., König, M., Janke, D., Hempel, S., Amon, T., 2018b. Investigation of discharge coefficient for wind-driven naturally ventilated dairy barns. Energy Build. 165, 132–140. https://doi.org/10.1016/j.enbuild.2018.01.038.

Zhang, G., Ikeguchi, A., Morsing, S., Takai, H., Ravn, P., Okushima, L., Bygholm, C., Agricultural, N., City, T., 2003. Obstacle Effects on Airflow and Contaminant Dispersion Around a Naturally Ventilated Livestock Building V, pp. 1–9.